JUEE

Journal of Urban and Environmental Engineering, v.16, n.1, p.15-24

ISSN 1982-3932
doi: 10.4090/juee.2022.v16n1.015024

**Journal of Urban and Environmental Engineering**

www.journal-uee.org

# CFD MODELING FOR PREDICTION OF $NO_X$ DISPERSION IN A STREET WITH ACTIVE PUBLIC URBAN INTERVENTION IN MEDELLÍN, COLOMBIA

Juan Felipe Rodriguez Berrio[1*], Carlos Alberto Riveros[2], Julio Cesar Saldarriaga[3], Jhon F. Hincapie[4] and Diego Hincapie Zuluaga[5]

[1]*Department of Escuela Ambintal, Universidad de Antioquia, Colombia*
[2]*Department of Escuela Ambiental, Universidad de Antioquia, Colombia*
[3]*Department of Escuela Ambiental, Universidad de Antioquia, Colombia*
[4]*Department of Ingenieria Mecanica, Universidad de Antioquia, Colombia*
[5]*Department of Ingenieria Mecanica, Instituto Tecnologico Metropolitano, Colombia*

Received 22 June 2021; received in revised form 25 March 2022; accepted 30 March 2022

**Abstract:** The Latin American and Caribbean (LAC) region suffers from persistent inequality, climate change vulnerabilityn and persistent air quality problems. The Aburrá Valley, Medellín, located in Colombia, is a narrow tropical valley with strong thermal inversion and unstable atmospheric conditions. In addition, local air pollutant concentration is strongly associated with Atmospheric Boundary Layer (ABL) variability. It is common to have in Medellín air quality episodes mainly exacerbated by the prolonged absence of precipitation. Although air pollution control strategies aimed at improving air quality have been recently implemented by the municipality of Medellín, values of $NO_2$ concentration remain unaltered during the last 8 years with values close to critical values. The present study analyzed a sensitive street in Medellín that has been subjected to recent public urban interventions with the construction of new public spaces and buildings without considering the effect of $NO_2$ concentration in planning such interventions. Therefore, it is expected to currently have areas in the urban area of Medellín with unhealthy $NO_2$ concentrations. This work addresses this problem by selecting an area of study in order to consider recent urban interventions conducted by the University of Antioquia, including new pedestrian areas in the context of $NO_x$ dispersion using CFD analysis. The numerical results allow the identification of low wind speed zones where $NO_x$ dispersion is also modeled.

**Keywords:** CFD; Air pollution; Traffic Emissions; Street Canyon; $NO_2$ concentration; ANSYS



**Nomenclatura**

$U_i$ Velocidad promedio
$\mu_t$ Viscosidad Turbulenta
$u_i$ velocidad fluctuante
$\omega$ Disyunción especifica
P Presión
$\Gamma_w \Gamma_k$ Difusividad Efectiva
$P_a$ Densidad
$p_{k_s}$ Turbulencia de vorticidad
$J_i$ Flujo de difusión
$C_\mu$ Constante emperica
$K_s$ Rugosidad de grano
$NO_2$ Dióxido de nitrógeno
K Constante de Von Karman
$y_o$ Parámetro de Rugosidad
$D_{\Im}$ Coeficiente de Difusión Másico
$S_{c_t}$ Numero de Schmidt turbulento
$\nu$ Velocidad de Fricción
$K(y)$ Energía Cinética Turbulenta
$\varepsilon(y)$ Tasa de Disipación Turbulenta
$NO$ Óxido nítrico
$C_s$ Constante Rugosidad
$\mu$ Viscosidad

* Correspondence to: Juan Felipe Rodriguez Berrio. E-mail: felipe.rodriguez@udea.edu.co

## INTRODUCTION

Air pollution poses a serious threat to public health, prolonged exposure to polluted air is responsible for approximately 4.2 million premature deaths worldwide and is expected to become the leading cause of death by 2050 (Gómez *et al.*, 2020, Lauriks *et al.*, 2021). In urban areas, human exposure to pollutants is high mainly due to the accumulation of traffic emissions primarily caused by a lack of sufficient ventilation. Therefore, enhancing pollution dispersion reduces pollutant exposure of pedestrians (Voodeckers *et al.*, 2021).

Vehicle exhaust emissions (especially those originating from diesel-powered vehicles) moderately contribute to the total mass of $PM_{2.5}$, but contain large amounts of fine particulate matter, nitrogen oxides ($NO_x$), and other toxic substances. Based on the study conducted by Brønnum-Hasen *et al.* 2018 in the Copenhagen Municipality, it was found that life expectancy increases in 0.3 years with a reduction of 20% exposure to $NO_2$, and a similar trend was observed in reducing incidence and prevalence of major chronic diseases. Considering the value of 6 $\mu g/m^3$ for rural $NO_2$ concentration used by Brønnum-Hasen *et al.* (2018), life expectancy is expected to increase by at least one year for men and half a year for women living in rural areas, compared to those in urban areas.

According to Zhao *et al.* (2021), $NO_2$ concentration is strongly correlated with mortality, and prolonged exposure to $NO_2$ causes mortality rates as great as those accounted for $PM_{2.5}$. Using data collected between 2014 and 2016 from the air pollution monitoring network of China in 31 provinces, Zhao *et al.* (2021) found that death rates from air pollution are highest for rural residents in developing countries mainly due to the use of traditional stoves for cooking and dependence on petroleum-based fuels. In contrast, developed countries have similar living standards in terms of essential factors, and therefore urban-rural differences solely depend on exposure to $NO_2$. Zhao *et al.* (2021) reported two $NO_2$ concentration critical values of 43 $\mu g/m^3$ and 48 $\mu g/m^3$ for increasing risk of cardiovascular and respiratory mortality, respectively. Finally, it is important to note that elderly residents and children in urban areas are most affected by $NO_2$ pollution, as highlighted by Zhao *et al.* (2021).

In recent years, several strategies have been proposed to reduce $NO_2$ pollution-related mortality. Fernández-Pampillón *et al.* 2021 conducted a field experiment in a medium-density urban neighborhood using Titanium Dioxide $TiO_2$ to reduce $NO_x$ pollution. A street located in the Municipality of Alcobendas (Spain) was selected as the photoactive zone having a size of 300 m long, and 36 m wide with an average height of 16 m. Fernández-Pampillón *et al.* (2021) concluded that no evident $NO_x$ remediation was detected in the photoactive zone. A complimentary study conducted by Sánchez *et al.* (2021), using Computational Fluid Dynamics (CFD) simulations, identified $NO_x$ emissions and wind flow as the most influential factors affecting the reduction of $NO_2$. Sánchez *et al.* (2021) found that lower wind velocities increase the residence time of pollutants, thus promoting the interaction between NO molecules and $TiO_2$. Additionally, an increase in $NO_x$ emissions causes an increase in $NO_2$ concentrations, which strongly depends on the traffic emission scenarios. Finally, Sánchez *et al.* (2021), based on CFD simulations, concluded that the use of $TiO_2$ in real applications only provides minimal reduction of $NO_2$ concentrations and increasing the photoactive surfaces must be carefully analyzed by considering the wind speed distributions in the area of analysis.

On the other hand, Lurkin *et al.* (2021) analyzed information from 257 Low Emission Zones (LEZs) in Europe and concluded that not only are operational rules important but also their interaction with road users. Lurkin *et al.* (2021) identified that in Europe, Italy is the leading country with 107 LEZs, followed by Germany with 82 LEZs. Although Lurkin *et al.* (2021) reported a significant reduction of $NO_2$ concentrations after the introduction of some LEZs, there are also reports without adequate support to validate the decrement of air pollution in some LEZs. Finally, Salas *et al.* (2021) assessed the effectiveness of a LEZ implemented in the center of Madrid (Spain), the selected LEZ corresponds to Plaza del Carmen, since the 1980s, Plaza del Carmen has no reported a value of $NO_2$ annual concentration lower than 40 $\mu g/m^3$. Therefore, using $NO_2$-level data from the air quality monitoring network of Madrid, collected during the period of December 2015 to May 2019, Salas *et al.* (2021) studied the effectiveness of the LEZ. The results show that the reduction of $NO_2$ concentrations in the Plaza del Carmen dropped to levels ranging from 23% to 34% after the introduction of the LEZ.

The Latin American and Caribbean (LAC) region suffers from persistent inequality, climate change vulnerability, and persistent air quality problems. Gómez Peláez *et al.* (2020) conducted a study to assess the air quality state between 2010 and 2017 in 11 metropolitan areas (MA) divided into three cities with more than 12 million inhabitants (Sao Paulo, Brazil; Buenos Aires, Argentina; Rio de Janeiro, Brazil), four cities with more than seven million inhabitants (Lima, Perú; Bogotá, Colombia; Santiago, Chile; Belo Horizonte, Brazil) and four cities with more than two million inhabitants (Valle de Aburrá, Medellín, Colombia; Vitória, Brazil; Quito, Ecuador; Salvador;

Brazil). Gómez Peláez *et al.* (2020) found that Santiago presented the long-term highest $NO_2$ concentration, followed by Medellín mainly due to thermal inversion and higher emissions. In Medellín, the annual concentration of $NO_2$ remains basically unaltered, showing a peak of 37.7 $\mu g/m^3$ ±8.3 $\mu g/m^3$.

The Aburrá Valley, Medellín, is a narrow tropical valley with strong thermal inversion and unstable atmospheric conditions. Herrera-Mejía and Hoyos, (2019) characterized the Atmospheric Boundary Layer (ABL) in the Aburrá Valley, Medellín, and found that when the average ABL height reaches its minimum (not exceeding the depth of the Aburrá Valley), unfavorable meteorological conditions facilitate unhealthy pollutant concentrations. Herrera-Mejía and Hoyos (2019) also found values of wind speed no larger than 3m/s inside the valley with higher values of wind speed of approximately 8 m/s at 2 km, which means considerably higher values of wind speed above the valley. Finally, Herrera-Mejía and Hoyos (2019) highlighted that "*the ABL height implicitly determines the pollutant concentration over time and space".*

Since vehicular emission is the main source of $NO_2$ in urban areas, finding locations where $NO_2$ pollution is stagnating, highly depends on traffic intensity, road configurations, and building heights. In addition, wind speed is strongly correlated to a higher dilution process. Therefore, it is important to consider urban geometry modifications on the wind flow in urban areas (Lauriks *et al.*, 2021).

The present study analyzed a sensitive street in Medellín that has been subjected to recent public urban interventions with the construction of new public spaces and buildings without analyzing the effect of $NO_2$ concentration in planning such interventions. The main objective of the study is to analyze the current situation in the street and surrounding areas in order to provide information to be considered in new public urban interventions, especially those that are currently under planning in areas of influence of the street.

Therefore, the dispersion of $NO_2$ and NO, present in the atmospheric air in that area of Medellín was simulated using CFD with the aim of predicting the concentrations of pollutants and velocity profiles at specific points within the study area. The simulations were performed using the ANSYS Fluent® software. The boundary conditions, wind speed, and the volumetric concentrations of the pollutants in the atmospheric air were obtained from two monitoring stations belonging to the Siata (Sistema de Alerta Temprana de Medellín y el Valle de Aburrá - https://siata.gov.co/) monitoring network, one to the north and the other to the south of the study area with the objective of validate the results obtained from the CFD simulation.

## MODEL SET-UP

The above-mentioned research findings showed the diverse factors to be considered when modeling $NO_2$ pollution. Aspects related to vehicle emissions, principles of $NO_2$ distribution in urban areas, wind speed distributions in the area of analysis, and, urban configuration. Akhatova *et al.* (2015), using CFD simulation, conducted a study of carbon monoxide (CO) dispersion in a crossroad street in Astana. Although the current level predicted by CFD simulations has not been achieved, the city is gradually reaching critical CO concentration levels. This situation is similar to the current situation in Medellin, where the annual concentration of $NO_2$ remains basically unaltered, showing a peak of 37.7 $\mu g/m3$ ±8.3 $\mu g/m^3$ (Gómez Peláez *et al.* 2020). It is important to note the $NO_2$ concentration critical values of 43 $\mu g/m^3$ and 48 $\mu g/m^3$ previously reported (Zhao *et al.* 2021). Finally, Akhatova *et al.* (2015) also stressed the fact that the accumulation of pollutants is precipitated by low wind conditions.

Lauriks *et al.*, (2021), using CFD simulation, also stressed the fact that the accumulation of pollutants is strongly heterogeneous and pollution hotspots are associated with areas where high buildings restrict natural ventilation. Thus, proper flow field and orography must be adequately determined when modeling pollutant dispersion in urban areas. Voodeckers *et al.* (2021) highlighted that CFD simulation is a powerful tool for modeling air quality in urban areas and adequate for predicting flow fields and dispersion patterns in urban areas.

Li *et al.* (2021) conducted a review on pollutant dispersion in urban areas studying research outputs from 219 references concluded that building opening should be larger than 20% and building separation should not be less than 10% to maintain good ventilation. Finally, Li *et al.* (2020) using CFD simulation and wind tunnel experiments found that the flow field at pedestrian level is highly correlated to street canyon configuration leading to better air quality at low wind speed (less than 1.4 m/s) when a step-down canyon is adopted.

### Study Area

The study area is made up of six blocks consisting of buildings of different heights and separated by streets. **Fig. 1** shows the aerial view, and **Fig. 2** shows the lateral view of the study area, respectively. It is possible to observe the university of Antioquia core research center (SIU for its Spanish acronym) in **Fig. 3.**

It is also possible to observe the Faculty of Medicine located in the N-E block (27m x 15,8m) and the Faculty of Odontology located in the N-W block just next to the Faculty of Medicine. Both faculties belong to the

university of Antioquia. The above-mentioned urban interventions were constructed during different periods of time in a residential area and were considered as individual units separated by public streets. It is also possible to observe the different architectural configurations adopted by the university of Antioquia for those interventions. To conduct the CFD simulation, the architectural details of the buildings considered in the study area were simplified using simple geometric figures for their representation. In this study, the main reference corresponds to the Faculty of Medicine and the SIU research center, which has a reference height H of 30 meters (**Fig. 3**).

Wind direction, as shown in **Fig. 3**, is defined perpendicular to the main building of the SIU research center in the N-S direction (greater prevalence of wind direction for the Aburrá Valley). The measurements of the concentration of atmospheric pollutants were obtained from the monitoring station 6 (Siata), located to the north and closest to the study area during three periods and for the entire month of April 2018. These recorded values were averaged to validate the computational model.

It is important to note that the street in the N-S direction is named Carabobo and has been subjected to different urban interventions. In the central area of Medellín, Carabobo street became, in recent years, a pedestrian street. Therefore, pollutants produced by vehicular combustion or accidental discharges in the area of study were not taken into account in the CFD model in order to study current pollutant dispersion in the street because there are plans to convert other portions of the Carabobo street (including the one considered in this study) into pedestrian street. In addition, the University of Antioquia is currently planning the construction of new infrastructure in the area of study in order to provide new research facilities to the SIU research center, urban intervention considers as well the construction of new pedestrian areas for users of the SIU research center.

**Fig. 1** Aerial view of the study area.

**Fig. 2** Lateral view of the study area.

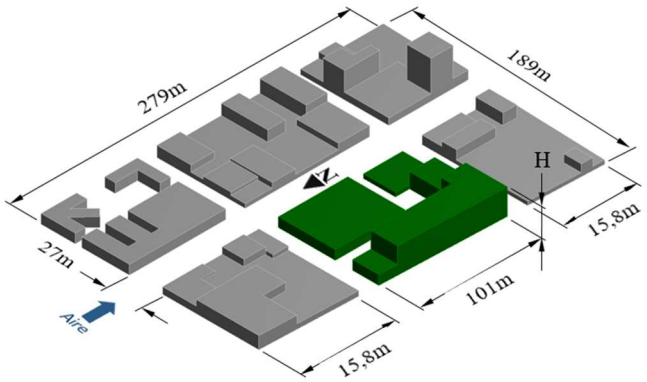


**Fig. 3** Study area model.

## Mathematical Model

The continuity and conservation of momentum equations are given by **Eq. (1)** and **(2)**, respectively.

$$\frac{\partial U_j}{\partial x_j} = 0, \tag{1}$$

$$\frac{\partial \rho U_j U_i}{\partial x_j} = \frac{-\partial P}{\partial x_i} + \frac{\partial}{\partial x_j}\left[(\mu + \mu_t)\left(\frac{\partial U_i}{\partial x_j} + \frac{\partial U_j}{\partial x_i}\right) - \rho\underline{u_i' u_j'}\right] + (\rho - \rho_{ref})g_i, \tag{2}$$

The instant velocity vector is given by $u_i = U_i + u_i'$, where $U_i$ is the average velocity $(m/s)$ and $u_i'$ is the fluctuatinng velocity $(m/s)$ in the direction $x_i$, $P$ is the pressure $(Pa)$, $\rho$ is the density of the fluid $(Kg/m^3)$, $\mu$ is the viscosity of the fluid $(Pa.s)$ and $\mu_t$ is the turbulent viscosity $(Pa.s)$. The value of the turbulent viscosity $\rho\underline{u_j' u_i'}$, is computed using the model SST $\kappa - \omega$ (Menter (1994), which combines the advantages of the models $\kappa - \omega$ y $\kappa - \varepsilon$, by employing mixing functions to solve the model $\kappa - \omega$ for the flow close to the wall and the model $\kappa - \varepsilon$ for the remaining flow. The turbulence model has to be modeled with the purpose to mathematically close the problem. The equations needed to model the turbulent kinetic energy $\kappa(Jkg^{-1})$ and the change of the specific dissipation $\omega$ $(s^{-1})$, are represented by **Eq. (3)** and **(4)**.

$$\frac{\partial(\rho U_j \kappa)}{\partial x_j} = \hat{P}_\kappa - \beta' \rho\kappa\omega + \frac{\partial}{\partial x_j}\left[\Gamma_\kappa \frac{\partial \kappa}{\partial x_j}\right] \tag{3}$$

$$\frac{\partial(\rho U_j \omega)}{\partial x_j} = \gamma \frac{\omega}{\kappa} P_\kappa - \beta' \rho \omega^2 + \frac{\partial}{\partial x_j}\left[\Gamma_\omega \frac{\partial}{\partial x_j}\right] + 2(1-F_1)\rho\sigma_{\omega 2}\frac{1}{\omega}\frac{\partial \kappa}{\partial x_j}\frac{\partial \omega}{\partial x_j}, \quad (4)$$

The effective diffusivity $\Gamma_\kappa$ y $\Gamma_\omega$ $(kgm^{-1}s^{-1})$ is given by **Eq. (5)** and **(6)**.

$$\Gamma_\kappa = \mu + \mu_t \sigma_\kappa, \quad (5)$$

$$\Gamma_\omega = \mu + \mu_t \sigma_\omega, \quad (6)$$

where $P_\kappa$ is the change of the production of turbulence due to viscous forces and buoyancy.

$$P_\kappa = \mu_t \frac{\partial U_i}{\partial x_j}\left(\frac{\partial U_i}{\partial x_j} + \frac{\partial U_j}{\partial x_i}\right), \hat{P}_\kappa = min(P_\kappa; C_1\varepsilon), \quad C_1 = 1.0. \quad (7)$$

In the model SST $\kappa - \omega$ the coefficients are expressed as follows: $\phi = F_1\phi_1 + (1-F_1)\phi_2$, where $\phi_1$ and $\phi_2$, are the coefficients of the models $\kappa - \omega$ and $\kappa - \epsilon$, respectively. The mixing functions are used to achieve a smooth transition between the models and the mixing functions $F_1$ and $F_2$, are computed from **Eq. (8)** and **(9)** as follows:

$$F_1 = tanh(arg_1^4), \text{con},$$

$$arg_1 = min\left[max\left[\frac{\sqrt{\kappa}}{\beta' \omega y}; \frac{500\nu}{y^2\omega}\right]; \frac{4\rho\sigma_{\omega 2}\kappa}{CD_{\kappa\omega}y^2}\right], \text{y},$$

$$CD_{\kappa\omega} = max\left[2\rho\sigma_{\omega 2}\frac{1}{\omega}\frac{\partial \kappa}{\partial x_j}\frac{\partial \omega}{\partial x_j}; 1.0e^{-10}\right], \quad (8)$$

where $y\ (m)$ is the closest distance to the wall.

$$F_2 = tanh(arg_2^2), \quad \text{with, } arg_2 = max\left[2\frac{\sqrt{\kappa}}{\beta' \omega y}; \frac{500\nu}{y^2\omega}\right]. \quad (9)$$

The turbulent viscosity is computed as follows:

$$\mu_t = \rho \frac{a_1 \kappa}{max(a_1\omega; \sqrt{2}SF_2)}, \text{con } a_1 = 0.31, \quad (10)$$

The magnitude of the vorticity is given by $S = \sqrt{S_{ij}S_{ij}}$ $(s^{-1})$, where $S_{ij} = \frac{1}{2}\left(\frac{\partial U_i}{\partial x_j} + \frac{\partial U_j}{\partial x_i}\right)$ $(s^{-1})$. All the constants included in the mixing functions are computed based on the constants from the models $\kappa - \omega$ y $\kappa - \epsilon$. The values used for the equation of turbulence are shown in **Table 1**.

**Table 1.** Valor de las constantes para el modelo de turbulencia SST $\kappa - \omega$, utilizadas en el análisis de dispersión de contaminantes ambientales.

| | | | | | |
|---|---|---|---|---|---|
| $\sigma_{\kappa 1}$ = 0.85 | $\sigma_{\omega 1}$ = 0.5 | $\beta_1$ = 0.075 | $\gamma_1$ = 0.5532 | $\beta'$ = 1.176 | $\beta_\infty$ = 0.03 |
| $\sigma_{\kappa 2}$ = 1.0 | $\sigma_{\omega 2}$ = 0.856 | $\beta_2$ = 0.0828 | $\gamma_2$ = 0.5532 | | |

The pollutant concentration is modeled using the Eulerian method in order to obtain the pollutant dispersion in the atmosphere. The convection-diffusion equation to compute the mass fractions of $Y_i$ $(kg/kg)$, is given by **Eq. (11).**

$$\frac{\partial}{\partial x_j}(\rho U_j Y_i) = \frac{\partial}{\partial x_j} J_i + S_i, \quad (11)$$

where $S_i$ is defined by the user $(kg/m^3.s)$, and $J_i$ corresponds to the diffusion part to be used in turbulent flow of $i$ and is computed using the **Eq. (12).**

$$J_i = \left(\rho D_{i,m} + \frac{\mu_t}{Sc_t}\right)\frac{\partial Y_i}{\partial x_j}, \quad (12)$$

Where $D_{i,m}$ is the mass diffusion coefficient of $Y_i$ in $(m^2/s)$, and $Sc_t$ is the turbulent Schmidt number, in the present work is defined as $Sc_t = 0.7$.

**Boundary Conditions**

Vertical air velocity, turbulent intensity, and specific dissipation rate as a function of height are used as boundary conditions in CFD simulations to define neutral atmospheric boundary layer flows. Therefore, there are two approaches typically used in CFD that describe the behavior of atmospheric boundary layer flows and therefore are used herein as boundary conditions at the entry of the domain. The approach put forward by Richards, P. J., and R. P. Hoxey (1993) and Architectural Institute of Japan (2004) are two widely used approaches. In this work, the Richards and Hoxey approach is adopted, assuming a vertical air velocity profile in flat terrain with constant shear stresses with height, as described in the **Eq. (13).**

$$u(y) = \frac{u}{\kappa} ln\left(\frac{y+y_0}{y_0}\right), \quad (13)$$

where $\kappa$, is the Von Karman constant, equals to 0.42, $y$ is the height coordinate, $y_0$ is the roughness parameter equals to 0.0033 $m$, and $u$ is the friction velocity obtained from the specific velocity $U_h = 1.04\,m/s$, at a height of $h = 10m$, as shown in **Eq. (14)**.

$$u = \frac{\kappa U_h}{ln((h+y_0)/y)}. \quad (14)$$

The vertical distribution of the turbulent kinetic energy is given by **Eq. (15).**

$$k(y) = \frac{u^2}{\sqrt{C_\mu}}, \quad (15)$$

where $C_\mu$ is an empirical constant equals to 0.09. The vertical profile of the turbulent dissipation rate is given by **Eq. (16)**.

$$\varepsilon(y) = \frac{u^3}{\kappa(y+y_0)} \quad (16)$$

In the turbulence model SST $\kappa - \omega$ adopted in the present work, the turbulent dissipation specific rate $\omega(y)$ must be provided, which is calculated from the turbulent kinetic energy $k(y)$ and the turbulent dissipation rate $\varepsilon(y)$, using **Eq. (17)**.

$$\omega(z) = \frac{\varepsilon(z)}{C_\mu k(z)} \quad (17)$$

Due to the fact that the air vertical velocity profile of gradually changes in the vicinity of walls as long as flow is moving downward, roughness modifications are needed in order to reproduce a gradual change in the air vertical velocity profile. Wall roughness is defined as wall functions in terms of sand grain roughness $k_s$, el parámetro de la longitud de rugosidad aerodinámica the aerodynamic roughness length parameter $y_o$ and the roughness constant $C_s$, required to the wall function as shown in **Eq. (18)**.

$$k_s = \frac{9.793 y_0}{C_s}, \quad (18)$$

Nevertheless, Blocken *et al.* (2007) recommend to consider the height of the sand grain roughness $k_s$, smaller than the height to the central point $P$ of the adjacent cell to the wall $z_p$, (inferior part of the domain), Therefor, the selected values in the present work based on the defined characteristics of the computational grid for each study case are $k_s = 0.064m$ y $C_s = 0.5$.

## Computational Domain

The computational domain used in the present work considers an upstream distance, between the inlet of the computational domain and the buildings, of 20H, to limit the development of the input gradients. The downstream distance, between the buildings and the outlet of the computational domain, corresponds to 60H. The lateral distances of the computational domain extended 16H, from the outer buildings to the lateral borders of the computational domain. The height of the computational domain is 8H, which is approximately equal to the height of the boundary layer of the terrain. The final dimensions of the computational domain are 1144 x 240 x 2678 [m] (X, Y, Z). Adequate modeling of the building area requires the definition of a subdomain in order to obtain greater precision in the solution. The dimensions of the computational subdomain are therefore 11H x 3H x 14H (X, Y, Z).

The computational domain and corresponding boundary conditions are shown in **Fig. 4.** To fully define the flow simulation, Dirichlet boundary conditions are set on the domain surfaces. For the upper border and the lateral borders of the domain, the symmetry condition is used, which considers a normal velocity and a gradient equal to zero in all the variables on the symmetry plane. For the exit boundary, an outflow condition was used, which considers that the flow is fully developed and the variables of interest do not change in the direction of the flow. For the floor and walls of buildings, a no-slip condition is implemented, which uses wall functions to consider the effect of roughness. Finally, for the input boundary of the computational domain, user-defined functions (UDF) are used to enter the profiles of velocity, turbulent kinetic energy and the turbulent dissipation rate as a function of the height of the domain, these aspects will be further discussed.

## Mesh Sensitivity Analysis

An adequate computational mesh is necessary in order to guarantee good representation of velocity profiles, concentrations of atmospheric pollutants around buildings, among other factors. The domain was discretized using the Cartesian Cut-Cell method. This method of mesh construction allows a better control of the size relationships, very fine meshes near the walls of the buildings to thicker meshes in the areas furthest from the area of interest as shown in **Fig. 4.** It is important to note that the size of the elements on the floor surfaces and the walls of the buildings are defined to comply with the value of $y^+ > 30$ in all mesh configurations.

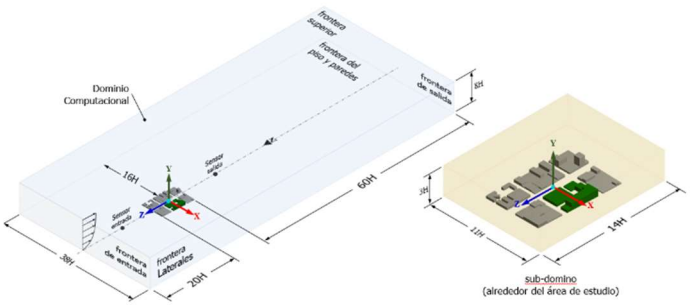


**Fig. 4** Computational domain and boundary conditions.

An analysis of mesh independence defined for the computational domain is performed using six mesh densities, which were generated in order to guarantee the mesh independence from the results obtained around the buildings. The north and south wind speeds were also considered in the sub-domain, on the Y-Z plane as shown in **Fig. 5.** Based on the above-mentioned, it was found that the speeds did not show significant changes when there are around 3.8 million elements in the domain. Therefore, this distribution provides a good balance between computational cost and numerical uncertainty.

## Physical Model

ANSYS Fluent® software is used to solve the RANS equations in steady state in three dimensions using the SST κ-ω turbulence model (Fluent, 2017). The SIMPLE algorithm is used for velocity-pressure coupling. An upwind second-order scheme is implemented for the convective term in order to improve the numerical precision, except for pressure. In addition, the convergence criterion is established when the residuals will reach a value equal to or less than $1x10^{-5}$, a value frequently reported in the literature. For all the case studies, about 2,100 iterations are required to obtain a convergence in the solution. The calculations are carried out on a parallel vector computer using sixteen Intel (R) Xeon (R) processors (CPUE5-2667 @ 2.90GHz) and 64Gb of RAM with a 64-bit operating system.

The validation of the CFD model was carried out by taking the mass fraction for $NO_2$ and NO at two points, one at the entrance and the other at the exit of the area of interest, and compared with the data reported by Siata. **Fig. 6** shows the validation of the computational model using the data provided by Siata. The standard deviation of the measurements collected in one month is calculated in order to determine the error. At the entrance of the computational domain, values of 6.693E-9 $\mu$g and 1.541E-8 $\mu$g are used, for NO and $NO_2$ respectively.

## Model Validation

On the other hand, values of 1.788E-8 $\mu$g and 1.984E-8 $\mu$g are used at the exit of the computational domain, for NO and $NO_2$, respectively. **Fig. 6** also shows good agreement between the experimental and CFD results at the entrance with a maximum relative error value of 2.95%. However, at the exit there is a relative error for nitric oxide of 8.11% and for nitrogen dioxide of 30.42%. The differences between the data reported experimentally and the data obtained in the CFD simulations is due, in large part, to atmospheric changes near the sites where the measurements were collected. Finally, the data entered into the computational model did not show these variations.

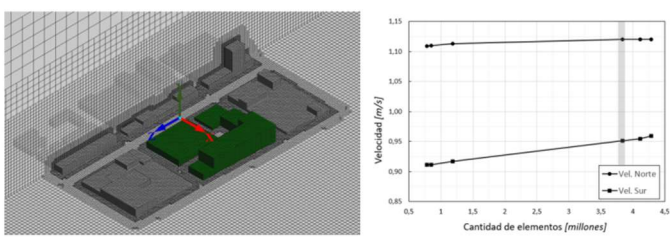


**Fig. 5** CFD model and north and south wind speeds.

## RESULTS

**Fig. 7** shows the wind flow field is represented by velocity vectors and velocity contours at a height of 2m in a horizontal section. It is also possible to observe that the highest wind speeds are parallel to the input wind speed. Recirculation vortices are present at road crossings, close to the intersections and parallel to the *x*-axis, this vortex is not present along the entire street. In the corner vortices there is a helical structure that transports the pollutants from the streets between the buildings to where the main wind flow is, parallel to the *z*-axis. It is important to note that the wind speeds along the *x* and *z* axes do not have a clear pattern along their path, due to the lack of uniformity in the shape and height of the buildings. Wind predominantly blows from north-south.

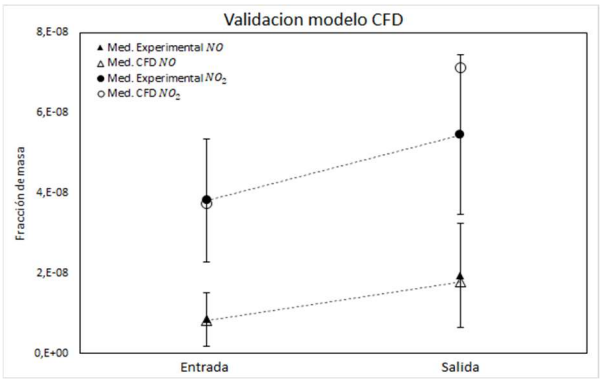


**Fig. 6** Place the caption below the drawing.

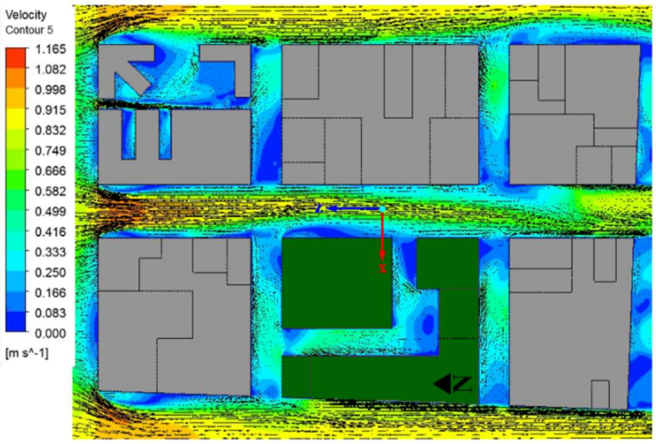


**Fig. 7** Wind flow field at a height of 2m in a horizontal section.

The average wind velocity at the pedestrian level drastically reduced in the west side of the street canyon right behind the Faculty of Medicine. The same pattern is also observed in SIU research center, especially in the pedestrian zone located in the east entrance of the SIU research center. **Fig. 8** shows the step-down street canyon right behind the Faculty of Medicine, Voodeckers *et al.* (2021) stated that the ratio of the building height to the street width (H/W ratio) also known as the Aspect Ratio (AR) has a threshold value of 0.65, values of AR larger than 0.65 produces sharp reduction of the pollutant exchange rate and ventilation capacity cannot be guaranteed. It is possible to observe in **Fig. 9** that the urban intervention conducted by the University of Antioquia using a configuration with AR>0.65 resulted in insufficient ventilation capacity in the step-down street canyon right behind the Faculty of Medicine.

Insufficient ventilation capacity is also observed in the pedestrian zone located in the east entrance of the SIU research center as shown in **Fig. 10 and 11**. Voodeckers *et al*. (2021) stated that the street canyon depth has a threshold value of 5.0, the SIU research center currently presents in some pedestrian zones values of AR larger than 5.0. Therefore, special measures have to be taken to ensure sufficient ventilation for new building construction in the SIU research center area. **Fig. 12** shows the horizontal section of $NO_x$ concentrations at a height of 2 m. It is possible to observe that $NO_x$ concentrations are larger in the above-mentioned areas where low wind speed was evident based on the simulation results.

Wind blows from north to south and therefore pollutants emitted from vehicles are dragging in that direction, but the situation is critical due to the fact that the two above-mentioned areas promote deposited $NO_x$. Sánchez *et al.* (2021) stated that lower wind speed increases the residence time of $NO_x$. Although no vehicle emissions are included in the CFD model presented in this paper, it is clear that even if the Carabobo street in the near future is defined as pedestrian-only use, special measures have to be taken to reduce the residence time of $NO_x$. considering the limitations of local mitigation approaches presented in this paper.

**Fig. 8** Faculty of Medicine (University of Antioquia).

**Fig. 9** Lateral view of the Faculty of Medicine (University of Antioquia).

**Fig. 10** SIU research center (University of Antioquia).

**Fig. 11** SIU research center side entrance (University of Antioquia).

In the central area of Medellín, some parts of the Carabobo street are defined as pedestrian-only use. Therefore, it is expected in the near future vehicle restriction access due to the active urban intervention that is currently under process in the area of study and the necessity to have areas for pedestrians. As previously mentioned, the Aburrá Valley, Medellín is a narrow tropical valley with strong thermal inversion and unstable atmospheric conditions. In addition, annual concentration of $NO_2$ remains basically unaltered in Medellín during the last 8 years showing a peak of 37.7 $\mu g/m^3$ ±8.3 $\mu g/m^3$, a value close to the findings of Zhao *et al.* (2021), who reported two $NO_2$ concentration critical values of 43 $\mu g/m^3$ and 48 $\mu g/m^3$ for increasing risk of cardiovascular and respiratory mortality, respectively. Therefore, public urban intervention must address full scale implementation of passive actions to control traffic-related air pollution, especially in areas that during the last years have been gradually converted in pedestrian areas. Finally, **Fig. 13** shows the concentration of $NO_2$ plus NO along the Y-Z plane, for different heights; Y=2, 5, 10 and 30 m. Due to the

diffusion phenomenon caused by turbulent vortices, the concentration of pollutants tends to be higher at ground level (Y=2 m). Akhatova *et al.* (2015) using CFD simulation conducted a study of carbon monoxide (CO) dispersion in a crossroad street in Astana and pointed out that pedestrians are exposed to higher CO concentration levels in comparison with inhabitants of buildings.

Finally, it is also possible to observe several trees located in the Faculty of Medicine. Benefits like cooling effects and energy saving are highlighted by Voodeckers *et al.* (2021). However, the simulation results presented in this paper show low wind speed areas and the corresponding increase of NO concentration in those areas. Considering the complex nature of deposited NOx, there is a possibility that vegetation in the area of the Faculty of Medicine increases NOx concentration. As reported by Voodeckers et al. (2021), negative effects due to trees in street canyons accounts for reduced wind speed and air exchange leading to increase of pollutant concentration depending on density and type of trees in street canyons.

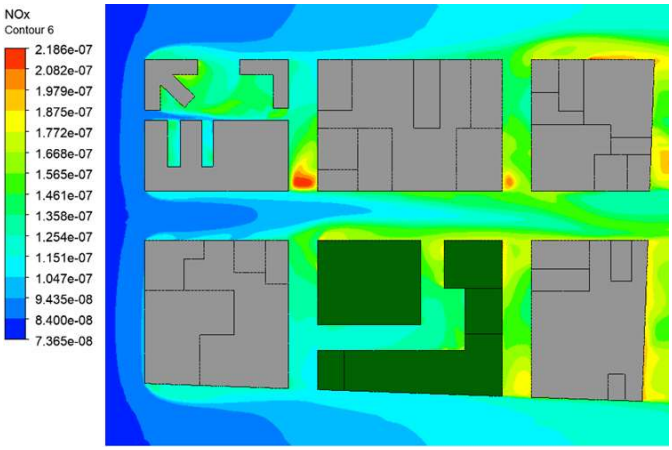


**Fig. 12** $NO_x$ concentrations at a height of 2m in a horizontal section.

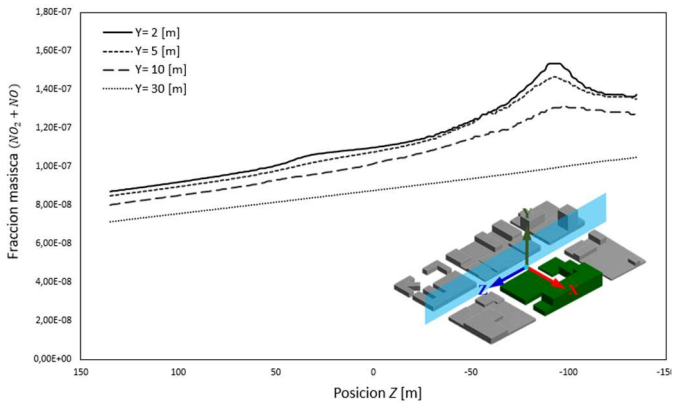


**Fig. 13** Concentration of $NO_2$ plus NO along the Y-Z plane.

## CONCLUSIONS AND REMARKS

This work aims to assessing current $NO_x$ dispersion in a street with active public urban intervention in Medellín, which is located in a narrow tropical valley with strong thermal inversion and unstable atmospheric conditions that facilitate unhealthy pollutant concentrations. Although annual concentration of $NO_2$ remains basically unaltered in Medellín during the last 8 years, measurements show values of $NO_2$ concentration close to critical values reported in the literature and due to the complex phenomenon associated to $NO_x$ dispersion, it is expected to currently have areas in the urban area of Medellín with unhealthy $NO_2$ concentrations. This paper address this problem by selecting an area of study in order to consider recent urban interventions conducted by the University of Antioquia including new pedestrian areas in the context of $NO_x$ dispersion.

The numerical results presented in this paper allowed the identification of low wind speed areas with increase of $NO_x$ concentration, those areas are expected to change to pedestrian-only use in the near future. Finally, although CFD is a powerful tool to study $NO_x$ dispersion in urban areas and the results presented in this paper are solely based on numerical results using data collected from Siata, there are several limitations in modeling local factors that probably affect the numerical results. Model calibration is important to validate simulation results. Therefore, it is recommended to conduct in-situ research to validate urban intervention developments during the design phase.

## REFERENCES

Gómez Peláez, L.M., Santos, J.M., Almeida Albuquerque, T.T., Costa Reis, N., Lemker Andreao, W. & Andrade, M.F. (2020) Air quality status and trends over large cities in South America. Environmental Science and Policy, 114, 422–435.

Brønnum-Hasen, H., Bender, A.M., Andersen, Z.J., Sørensen, J., Hjort Bønløkke, J., Boshuizen, H., Becker, T., Diderichsen, F. & Loft, S. (2018) Assessment of impact of traffic-related air pollution on morbidity and mortality in Copenhagen Municipality and the health gain of reduced exposure. Environment International, 121, 973–980.

Herrera-Mejía, L. & Hoyos, C.D. (2019) Characterization of the atmospheric boundary layer in a narrow tropical valley using remote-sensing and radiosonde observations and the WRF model: the Aburrá Valley case-study. Quarterly Journal of the Royal Meteorological Society, 2019, 1–25.

Lauriks, T., Longo, R., Baetens, D., Derudi, M. Parente, A., Bellemans, A. Beeck, J. & Denys, S. (2021) Application of improved CFD modeling for prediction and mitigation of traffic-related air pollution hotspots in a realistic urban street. Atmospheric Environment, 246, 118127.

Li, Z., Zhang, H., Wen, C.Y, Yang, A.S. & Juan, Y.H. (2020) Effects of height-asymmetric street canyon configurations on outdoor air temperature and air quality. Building and Environment, 183, 107195.

Li, Z., Ming, T., Liu, S., Peng, C., Richter, R., Li, W., Zhang, H. & Wen, C.H. (2021) Review on pollutant dispersion in urban areas-part A: Effects of mechanical factors and urban morphology. Building and Environment, 190, 107534.

Lurkin, V., Hambuckers, J. & Woensel, T. (2021) Urban low emissions zones: A behavioral operations management perspective. Transportation Research Part A, 144, 222-240.

Fernández-Pampillón, J., Palacios, M., Núñez, L., Pujadas, M., Sanchez, B., Santiago, J.L. & Martilli, A. (2021) NOx depolluting performance of photocatalytic materials in an urban area – part I: monitoring ambient impact. Atmospheric Environment, https://doi.org/10.1016/j.atmosenv.2021.118190.

Salas, R., Perez-Villadoniga, M.J., Prieto-Rodriguez, J. & Russo, A. (2021) Were traffic restrictions in Madrid effective at reducing NO2 levels?. Transportation Research Part D, 91, 102689.

Sanchez, B., Santiago, J.L., Martilli, A., Palacios, M., Núñez, L., Pujadas, M. & Fernández-Pampillón, J. (2021) NOx depolluting performance of photocatalytic materials in an urban area - Part II: assessment through Computational Fluid Dynamics simulations. Atmospheric Environment, 246, 118091.

Voordeckers, D., Lauriks, T., Denys, S., Billen, P. Tytgat, T. & Van Acker, M. (2021) Guidelines for passive control of traffic-related air pollution in street canyons: An overview for urban planning. Landscape and Urban Planning, 207, 103980.

Akhatova, A., Kassymov, A., Kazmaganbetova, M. & Rojas-Solórzano, L. (2015) CFD simulation of the dispersion of exhaust gases in a traffic-loaded street of Astana, Kazakhstan. Journal of Urban and Environmental Engineering, 9(2), 158166.

Zhao, S., Liu, S., Hou, X., Sun, Y. & Beazley, R. (2021) Air pollution and cause-specific mortality: A comparative study of urban and rural areas in China. Chemosphere, 262, 127884.